minerals

MDPI

Article

Influence of Layered Angle on Dynamic Characteristics of Backfill under Impact Loading

Jinxin Li [1,2], Wei Sun [1,2,*], Qiqi Li [1,2], Shuo Chen [1,2], Mingli Yuan [1,2] and Hui Xia [1,2]

[1] Faculty of Land and Resources Engineering, Kunming University of Science and Technology, Kunming 650093, China; 20192201108@stu.kust.edu.cn (J.L.); 20192239011@stu.kust.edu.cn (Q.L.); 20192201114@stu.kust.edu.cn (S.C.); 20192201138@stu.kust.edu.cn (M.Y.); 20192101091@stu.kust.edu.cn (H.X.)
[2] Yunnan Key Laboratory of Sino-German Blue Mining and Utilization of Special Underground Space, Kunming 650093, China
* Correspondence: kmustsw@kust.edu.cn

Abstract: In order to explore the relationship between the filling surface angle and the dynamic characteristics of the filling body under impact load, this paper uses the Hopkinson pressure bar (SHPB) test system to study the influence of different filling surface angles, different cement–sand ratios and different strain rates on the dynamic peak strength, dynamic strength growth factor and failure mode of the filling body. The results show that with the increase in the average strain rate, the dynamic peak strength and dynamic strength growth factor of the layered filling body increase gradually. With the increase in the filling surface angle, the static and dynamic peak strength of the layered filling body decreases gradually, but there is no obvious change law linking the dynamic strength growth factor and filling surface angle. According to the failure mode analysis and the LS-DYNA numerical simulation results for the layered filling body, with the increase in the filling surface angle, the failure mode of the layered filling body changes from splitting failure under tension to shear failure. The research results in this paper can provide theoretical support for the stability of underground layered filling bodies.

Keywords: layered filling body; filling surface angle; dynamic peak strength; static peak strength; dynamic strength increase factor

Citation: Li, J.; Sun, W.; Li, Q.; Chen, S.; Yuan, M.; Xia, H. Influence of Layered Angle on Dynamic Characteristics of Backfill under Impact Loading. *Minerals* **2022**, *12*, 511. https://doi.org/10.3390/min12050511

Academic Editors: Yanli Huang, Junmeng Li and Abbas Taheri

Received: 22 March 2022
Accepted: 18 April 2022
Published: 20 April 2022

1. Introduction

With the depletion of shallow mineral resources, resource exploitation gradually develops toward deeper ones [1–3]. In order to satisfy the development trend of the mining industry in this new situation, major mining enterprises are committed to seeking new ideas, concepts and technologies for the coordinated development of the economy, the environment and resources. Therefore, ensuring the green and coordinated sustainable development of metal mines has become a research hotspot for scholars both nationally and internationally [4–6]. However, with the increase in mining depth, high ground stress and high temperature have become especially serious [7,8], and the large amount of solid waste, such as tailings and waste rock, accompanying the ore output also affects the green development concepts of mining enterprises. Therefore, the backfill mining method has become an important method for safe and green mining of deep resources [9–11].

As an important part of the efficient application of the backfill mining method, the strength value of the backfill has been studied by scholars nationally and internationally. Zhou et al. [12] used a combination of physical experiments and mathematical models to obtain the effects of different curing ages on the compressive strength of the backfill and deduced three time-dependent mathematical models to characterize the effects of the cement–sand ratio and concentration value on the peak strength of the backfill. Zhang et al. [13] used a low-field NMR system to test the hydration time of the slurry in order to investigate the effect of different water-reducing agent additions on the peak strength and

slurry consistency of backfill, and the results showed that the addition of water-reducing agents improved the fluidity of the slurry and increased the strength value of backfill. Xv et al. [14] used indoor experiments to study the different effects of fiber doping on the peak strength and deformation modulus of the backfill. The results showed that with the increase in fiber content, the peak strength of backfill showed a trend the changed from increasing to decreasing. Cao et al. [15] investigated the effect of fiber type and fiber admixture on the early strength of backfill and prepared backfill specimens with different cement-tailing ratios, different curing ages and different fiber admixtures, then measured their uniaxial compressive strength. The results showed that the addition of fibers improves the uniaxial compressive strength of backfill and enhances its crack resistance. Kesimal et al. [16], in order to investigate the influence of different types of sulfur-containing tailings on the peak strength of the backfill, tested the strength values of backfill containing different tailings, and the results showed that the physical and chemical properties of tailings have some influence on the peak strength of backfill. However, during the underground mining process, the backfill is affected by the impact load brought by the blasting of underground ore in addition to the quasi-static load generated by the rock shift of the overlying rock layer. Xue et al. [17] applied the Hopkinson pressure bar test system and a high-speed camera to perform kinetic tests on backfill containing polypropylene fibers, and the results showed that the addition of fibers could cause a double-peak phenomenon in the dynamic stress–strain curve of the backfill. Song et al. [18] applied the SHPB test system to perform uniaxial impact experiments on backfill with different straw contents in order to improve the kinetic properties of the backfill, investigating the relationship between the straw content and the dynamic peak intensity of the backfill. The results showed that the addition of straw could improve the dynamic peak strength of the backfill.

Due to the limitations of current filling capacities, it is difficult to complete the backfill of large-scale goafs with a single filling, as this would lead to an obvious layered structure in the solidified backfill [19]. Wang et al. [20] investigated backfill containing different layered structures by means of uniaxial compression experiments and an acoustic emission monitoring system to explore the relationship between the strength values of layered backfill and the number of layers. The results showed that the presence of layers resulted in a certain weakening effect on the uniaxial compressive strength of the backfill. Liu et al. [21] investigated the kinetic properties and static parameters of double-layered backfill with various concentrations and cement-tailing ratios by means of Hopkinson pressure bar and uniaxial compression experiments, and the results showed that the failure mode of double-layered backfill mainly depends on the layer with the lower strength. Wang et al. [22] investigated the strength value properties of layered backfill by means of triaxial cyclic loading and unloading equipment. The results showed that the peak strength of backfill gradually increases with increases in surrounding pressure.

The reasons for filling-surface formation are mainly related to the following two factors. The first is the bleeding segregation of slurry. When filling slurry is filled into a goaf through a pipeline, the coarse aggregates in the slurry first sink at the pipe mouth while the fine aggregates continue to flow forward and sink far from the pipe mouth, resulting in the formation of a filling surface with a certain angle after solidification [23]. Second, the filling times of slurry—which mean that, with many open stopes, the filling stope area can reach hundreds of thousands of m^3, depending on the filling slurry ability—inevitably cause the phenomenon of solidified filling body stratification. Therefore, in this paper, the influences of the filling surface angle, the cement–sand ratio and different strain rates on the dynamic characteristics and failure mode of layered backfill were studied using an SHPB test system and LS-DYNA simulation software.

2. Experiment

2.1. Specimen Preparation

2.1.1. Experimental Materials

The tailings used in the experiment were taken from the unclassified tailings of a gold mine in Yunnan Province. The size composition curve of the tailings is shown in Figure 1, and the chemical constituents of the tailings are shown in Table 1. It can be seen from Figure 1 that the content of −200 mesh in the tailings was 70.13%, the content of −20 μm fine particles was 30.15% and the average particle size d was 40.93 μm. The cement used in the test was PC32.5R slag–Portland cement, and the test water was ordinary tap water.

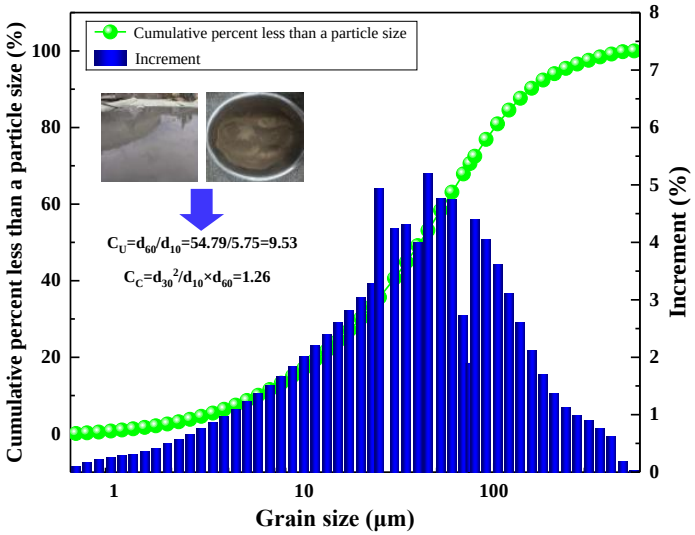

Figure 1. Composition curve of total tailings.

Table 1. Chemical constituents of tailings.

Component	CaO	MgO	SiO_2	Al_2O_3	S	Cu	Zn	TFe
Content/%	5.96	2.08	45.89	12.32	0.5	0.035	0.067	11.06

2.1.2. Experimental Protocol

This experiment used mold-pouring specimens with a diameter of 50 mm × 25 mm, with two pouring times and a pouring interval of 24 h. In laboratory conditions, the mold was placed, after one-layer casting, on a wood board with a calculated angle (0°, 5° and 13°). After one-layer curing, the wood board was removed and the second layer was poured. After two-layer curing, a filling surface with a certain angle was obtained. The mass concentration of the slurry was 68% and the ratios of cement to sand were 1:4, 1:6 and 1:8, as shown in Figure 2. Since the SHPB test system has a certain discreteness, 33 specimens (including three 50 mm × 100 mm specimens; the static peak strength was tested by uniaxial pressing) were poured with each ratio, as shown in Figure 3. The concrete pouring scheme used in the experiment is described in Table 2.

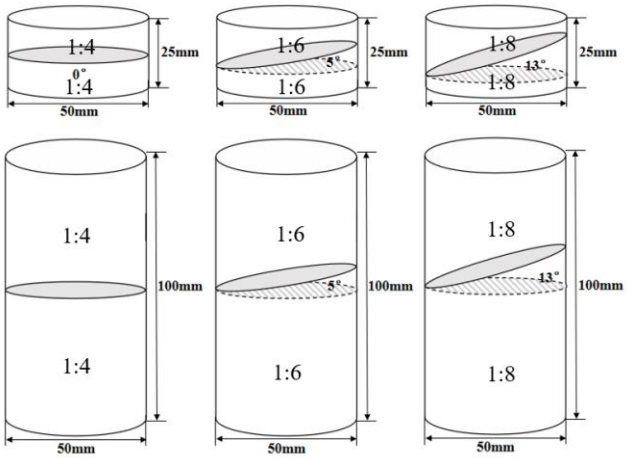

Figure 2. Schematic diagram of layered backfill specimens.

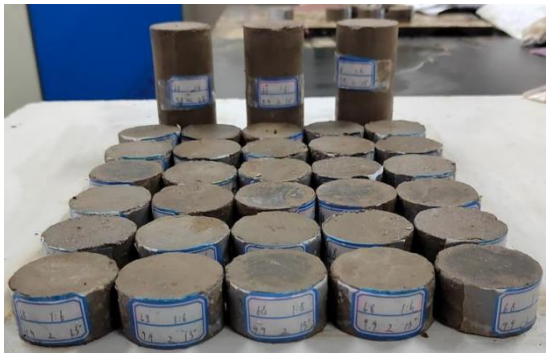

Figure 3. Partial test specimens.

Table 2. Specimen pouring scheme.

Layer Number	Mass Concentration/%	Cement–Sand Ratio	Angle/°	Impact Pressure/MPa
2	68	1:4/1:4	0	0.20; 0.21; 0.23; 0.25; 0.27
		1:4/1:4	5	
		1:4/1:4	13	
		1:6/1:6	0	
		1:6/1:6	5	
		1:6/1:6	13	
		1:8/1:8	0	
		1:8/1:8	5	
		1:8/1:8	13	

2.1.3. Experimental Method

Following the scheme described in Table 2, the prepared slurry was poured into the mold interior and then the slurry pouring amount was determined according to the internal calibration value of the mold. After the first layer of pouring was completed, the second layer was continuously poured at an interval of 24 h. The pouring amount of the second layer was greater than the height of the mold. After the initial setting of the slurry, the slurry with more holes in the upper part of the mold was scraped with a scraper. After 24 h, the mold was removed. The specimen removed was put into a humidity curing box at a constant temperature for 28 d. After reaching the curing age, the lower surface of the specimen was polished with sandpaper so that the specimen had high flatness. The specifics of the experimental method are shown in Figure 4.

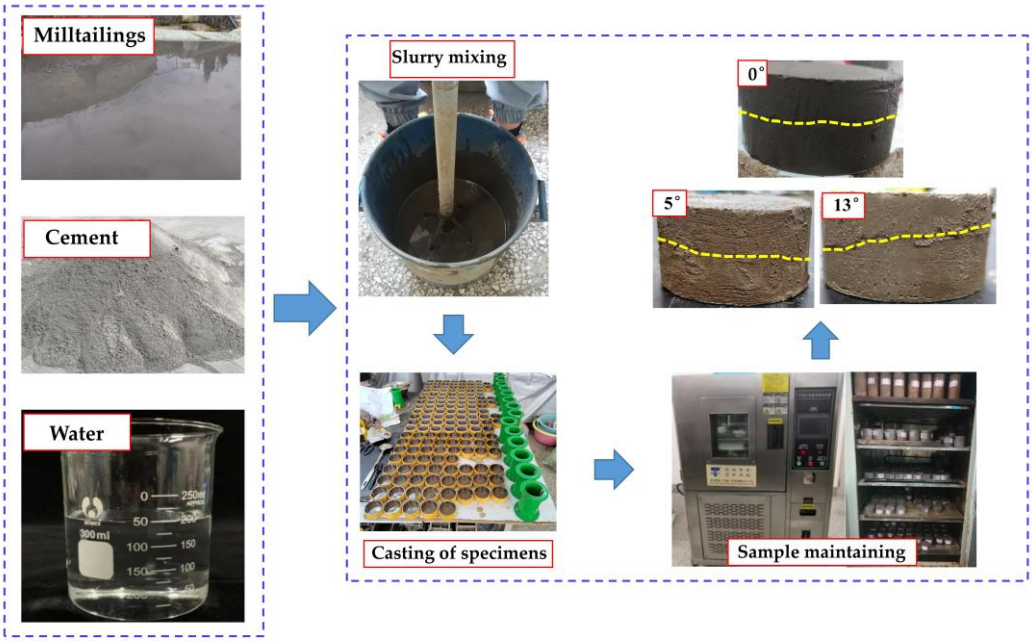

Figure 4. Preparation of stratified backfill specimen.

2.2. SHPB Device

The uniaxial impact test of the layered filling body was carried out using an SHPB test system with a diameter of 50 mm, and the effects of the strain rate, cement–sand ratio and filling surface angle on the dynamic characteristics of the filling body were studied. The length of the entry and transmission rod was 2.5 m with a diameter of 50 mm. The length of the impact rod was 0.4 m and the shape was a spindle. The rod material was alloy steel with a density of 7800 kg/m^3, elastic modulus of 210 GPa and Poisson's ratio of 0.25~0.3. The strain signal was collected and recorded by the foil strain gauge. The sensitivity coefficient of the strain gauge was 2.08 and its resistance was 120 Ω; the model was BFH120-5AA-D-D150 and the accuracy grade was A. The impact pressure was set to 0.20, 0.21, 0.23, 0.25 and 0.27 MPa. Before the beginning of the experiment, the normal connection of each circuit was checked, and an air-impact experiment was used to determine whether the system was in a normal working state. The experimental device is shown in Figure 5.

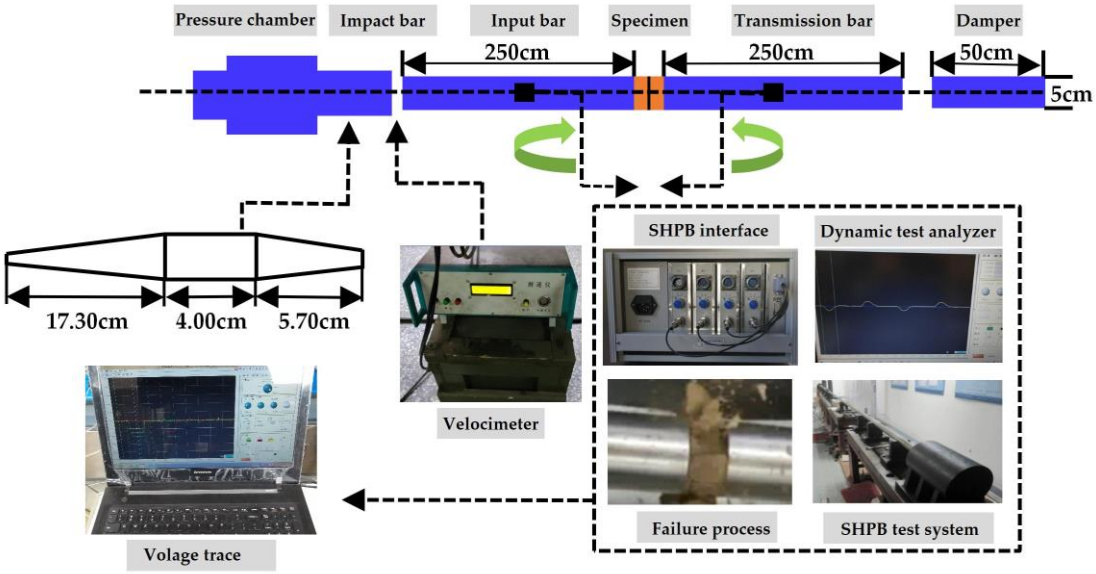

Figure 5. Structure of the SHPB test system.

3. Outcome and Discussion

3.1. Voltage Signal Curve of Layered Filling Body

According to the principle of the SHPB experiment, a three-wave method is generally used to test whether the internal stress of the specimen is uniform [24]. As shown in Figure 6a, when the mass concentration of the layered filling body is 68%, the average strain rate is 24.74 s^{-1}, the cement–sand ratio is 1:4, the number of layers is two and the angle of the layers is 5°. The incident wave and the reflected wave of the filling body are basically equal to the transmitted wave. Therefore, the stresses on both ends of the specimen before impact crushing are basically the same, thus meeting the macroscopic equilibrium conditions.

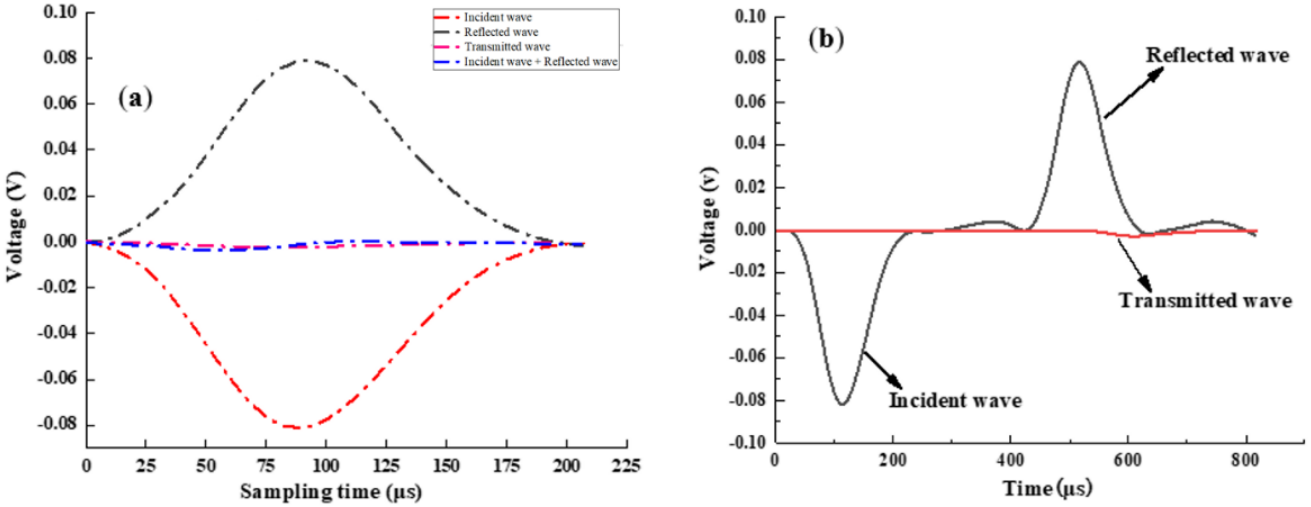

Figure 6. Voltage signal curve and stress balance test of a layered filling body: (**a**) stress balance test; (**b**) voltage signal curve.

Figure 6b shows the typical signal curve of a layered filling body. It can be seen that the incident and reflected wave peaks of the filling body are basically the same and the opposite amplitudes of the two directions are consistent, while the amplitude of the transmitted wave is relatively small. Since the filling body belongs to a heterogeneous body with a large number of pore structures, its wave impedance is much smaller than that of the steel rod. When the stress wave acts on the filling body interface, most of the stress wave returns to the incident rod and only a small number of stress waves are transmitted to the transmission rod, so the amplitude of the transmission wave is small. Therefore, the filling body has a strong damping effect on the propagation of the stress wave [25].

3.2. Dynamic Stress–Strain Curves of Layered Filling Body

As shown in Figure 7, when the stratification angle was 5° and the cement–sand ratio was 1:4, the dynamic peak strength of the layered filling body gradually increased with the increase in the impact rate. However, there was a certain oscillation in the dynamic stress–strain curve obtained from the experiment, which was mainly related to the internal pore structure and the strength value of the filling body [26]. When the average strain rate was 24.74 s^{-1}, the AB section in Figure 7 indicates the linear elastic deformation stage. There were no micro-pores or micro-cracks in the filling body, and the specimen had high integrity. The value range of σ in this stage was $0 < \sigma < \sigma_t$; σ_t is the crack initiation value, which can also be regarded as the starting point of the plastic deformation stage of the filling body. The value is generally about 70% of the dynamic peak strength of the filling body. The BC section indicates the plastic deformation stage, when the micro-pores and micro-cracks in the filling body develop rapidly and it is penetrated with new cracks. With the extension of the action time, the degree of damage to the filling body gradually intensified, with a value range of σ between $\sigma_t < \sigma < \sigma_p$; σ_p is the dynamic peak strength of the filling body. The section CD indicates that when $\sigma_p < \sigma$, the specimen entered the post-peak failure

stage and the primary cracks and new cracks rapidly intersected and penetrated to form a macro-failure surface, while the specimen basically lost its bearing capacity [27].

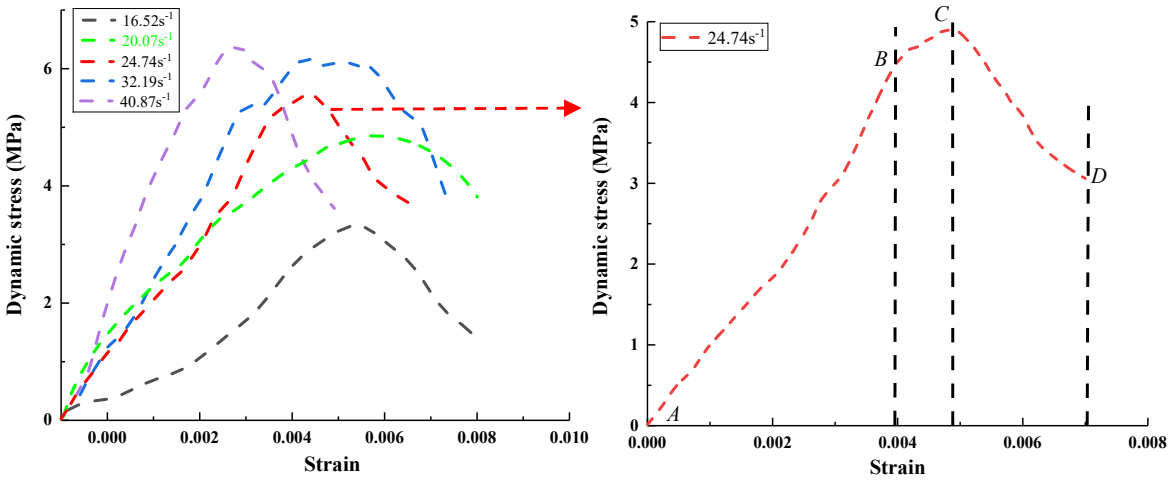

Figure 7. Dynamic stress−strain curve of layered filling body.

3.3. Influence of Average Strain Rate on Dynamic Characteristics of Layered Filling Body

Figure 8 shows the variation curve of the dynamic peak strength of layered backfill with the average strain rate when the layered angle was 5°. It can be seen that with the increase in the average strain rate, the dynamic peak strength of the layered backfill with a cement–sand ratio of 1:8 increased from 1.17 MPa to 1.83 MPa. The dynamic peak strength of the layered backfill with a cement–sand ratio of 1:6 increased from 1.74 MPa to 3.82 MPa, and the dynamic peak strength of the layered filling body with a cement–sand ratio of 1:4 increased from 3.64 MPa to 6.35 MPa. Therefore, with the increase in the average strain rate, the dynamic peak strength of the layered filling body increased gradually. When the incident wave acts on the interface of the filling body, the stress wave transmitted into the filling body generates an energy concentration in the delamination and the pore structure of the filling body. Due to the low energy dissipation rate of the filling body, it is impossible to achieve energy dissipation by only increasing its own stress to resist the energy generated in the pore structure of the specimen. With the increase in the cement–sand ratio, the dynamic peak strength of the filling body increased gradually, mainly because the internal structure of the filling body with more cement content was more dense and more energy was needed to cause the failure and instability of the filling body.

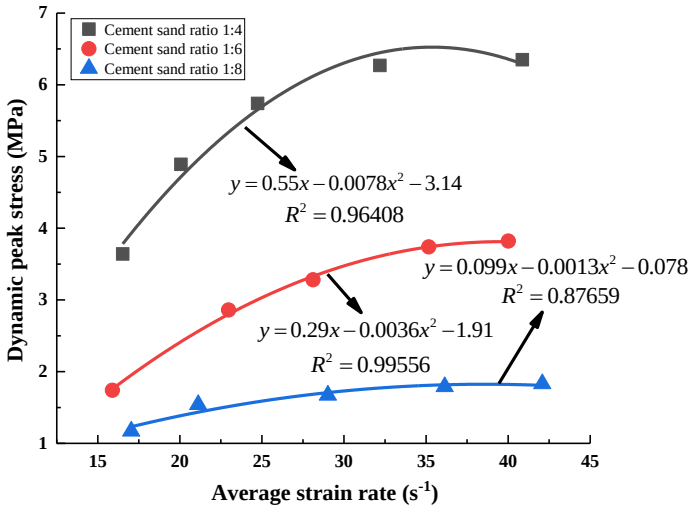

Figure 8. Relationship between average strain rate and dynamic peak stress.

As shown in Figure 9, the static peak strength of the layered filling body decreased with the decrease of the cement–sand ratio. As shown in Figure 10, the dynamic strength growth factor of the filling body was calculated using the static peak strength to determine the dynamic compression characteristics of the filling body. When the cement–sand ratio was 1:4, the dynamic strength growth factor of the backfill increased from 2.00 to 3.95 with the increase in the average strain rate; when the cement–sand ratio was 1:6, the dynamic strength growth factor of the filling body increased from 2.38 to 5.23; when the cement–sand ratio was 1:8, the dynamic strength growth factor of the filling body increased from 2.09 to 3.27. Therefore, with the increase in the average strain rate, the dynamic strength growth factor of the filling body increased gradually, and the dynamic strength growth factor of the filling body with the cement–sand ratio of 1:6 was greater than those of the filling bodies with the cement–sand ratios of 1:4 and 1:8.

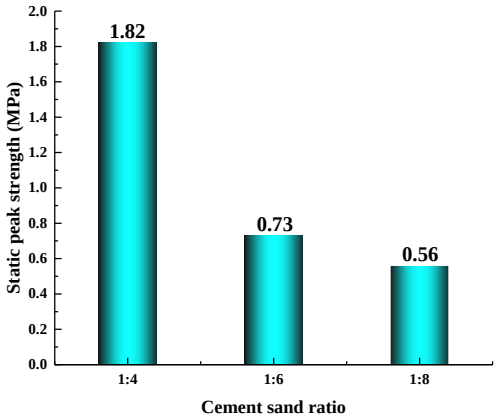

Figure 9. Relationship between cement−sand ratio and static peak strength.

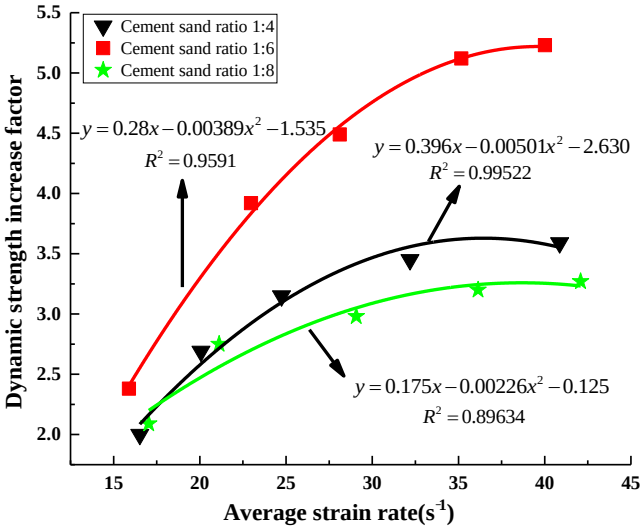

Figure 10. Relationship between dynamic strength growth factor and average strain rate.

3.4. Influence of Angle of Filling Surface on Dynamic Characteristics of Filling Body

As shown in Figure 11, when the approximate strain rate was 41 s^{-1} (as the accurate strain rate of the filling body was uncontrollable, the approximate strain rate was adopted), the dynamic peak strength of the layered filling body with the cement–sand ratio of 1:4 decreased from 7.39 MPa to 4.96 MPa with the increase in the filling surface angle. The dynamic peak strength of the layered filling body with the cement–sand ratio of 1:6 decreased from 3.95 MPa to 3.17 MPa, and the dynamic peak strength of the layered filling body with the cement–sand ratio of 1:8 decreased from 1.86 MPa to 1.54 MPa. Therefore, with the increase in the stratification angle, the dynamic peak strength of the filling body

gradually decreased. The main reason was that the micro-cracks in the filling surface were greater than the micro-cracks in the complete filling body because the bonding of the filling surface of the layered filling body was far lower than that of the complete filling body. When the angle of the filling surface increases to a certain extent, it is easy for the micro-cracks in the filling body to expand along the tip, which may produce stress concentration resulting in the failure of the layered filling body along the filling surface. Therefore, the dynamic peak strength of the layered filling body decreased gradually with the increase in the angle of the filling surface.

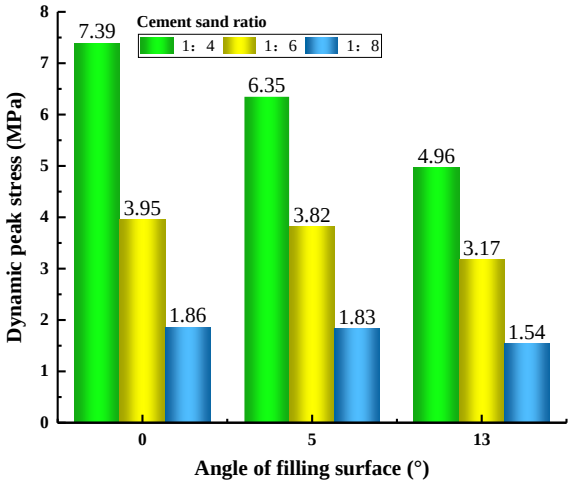

Figure 11. Relationship between angle of the filling surface and the dynamic peak strength.

As shown in Figure 12, the static peak strengths of layered fillings with different cement–sand ratios decreased with the increase in the filling surface angle. As shown in Figure 13, the dynamic strength growth factor of the filling body was calculated using the static peak strength. With the increase in the angle of the filling surface, the dynamic strength growth factor of the layered filling body with the cement–sand ratio of 1:4 increased from 3.99 to 4.10. The dynamic strength growth factor of the layered filling body with the cement–sand ratio of 1:6 decreased from 5.20 to 4.66. The dynamic strength growth factor of the layered filling body with the cement–sand ratio of 1:8 increased from 3.26 to 4.16. Therefore, according to the above analysis, with the increase in the filling surface angle, the dynamic strength growth factor of the layered filling body showed no obvious change.

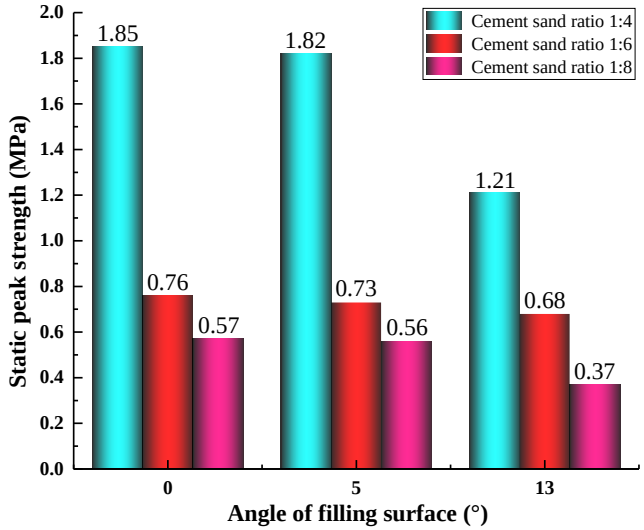

Figure 12. Relationship between the angle of the filling surface and the static peak strength.

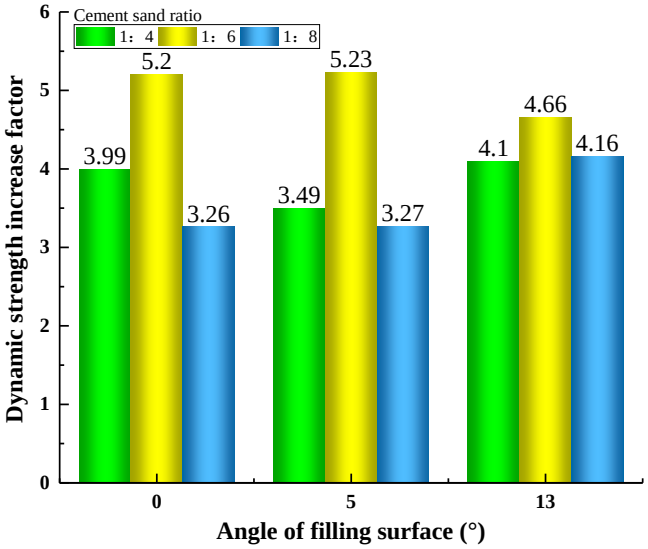

Figure 13. Relationship between the angle of the filling face and the dynamic strength growth factor.

4. Failure Mode Analysis of Layered Filling Body

As shown in Figure 14a, when the approximate strain rate was 16 s^{-1}, the cement-tailing ratio was 1:4 and the angle of the filling surface was 0°, there was no obvious damage in the upper and lower layers of the filling body but fractures occurred along the middle of the specimen. Due to the existence of the filling body's filling surface, the stress wave transmitted into the filling body continued to reflect and transmit in the stratification of the specimen, which intensified the dynamic process in the stratification. This resulted in the splitting failure of the specimen under the action of tension along the filling surface. When the angle of the filling was 5°, the layered filling body was slightly damaged along the middle filling surface and many through cracks were produced along the axial direction, but the specimen still had a high bearing capacity. When the angle of the filling surface was 13°, the failure mode of the layered filling body was quite different from the filling bodies with 0° and 5°. The failures of 0° and 5° filling bodies were mainly related to splitting failures along the filling surface of the specimen, while the failure of the 13° filling body mainly concerned shear failure along the filling surface of the specimen. Therefore, under the impact load, with the increase in the angle of the filling surface, it was easy for the layered filling body to slip along the filling surface, resulting in the loss of the bearing capacity of the filling body.

As shown in Figure 14b, when the approximate strain rate was 27 s^{-1} and the cement-tailing ratio was 1:4, the degree of damage to the filling body gradually intensified when the angle of the filling surface was 0°, and the upper and lower layers were seriously damaged along the axial direction. The main reason was that when the stress wave acts on the interface of a filling body, the Poisson effect leads to a large tensile stress along the transverse direction of the impacted specimen. Therefore, the filling body specimen was seriously damaged along the axial direction. When the angle of filling surface was 5°, the layered filling body was seriously damaged along the circumferential direction, but the specimen still had a certain bearing capacity. When the angle of the filling surface was 13°, the layered filling body was fractured along the axial direction, and more filling body blocks were produced.

As shown in Figure 14c, with an approximate strain rate of 40 s^{-1} and a cement-tailing ratio of 1:4, the 0°, 5° and 13° filling bodies were completely broken and lost their bearing capacities.

Figure 14. Influence of different filling surface angles on the failure mode of a layered filling body: (**a**) failure mode of layered filling body with approximate strain rate of 16 s^{-1}; (**b**) failure mode of layered filling body with approximate strain rate of 27 s^{-1}; (**c**) failure mode of layered filling body with approximate strain rate of 40 s^{-1}.

5. Numerical Simulation of Dynamic Mechanical Properties of Filling Body

5.1. Finite Element Model

ANSYS/LS-DYNA software was used to simulate the dynamic response mechanism of a layered filling body under impact load. The length of the transmission rod was 2.5 m, the diameter was 50 mm, the shape of the punch was spindle-shaped and the angles of the test piece were 0°, 5 ° and 13°. Since the specimen and the rod were both cylinders, the grid division was carried out using *hex and the spindle-shaped punch was divided with a free grid. The resulting finite element model is shown in Figure 15.

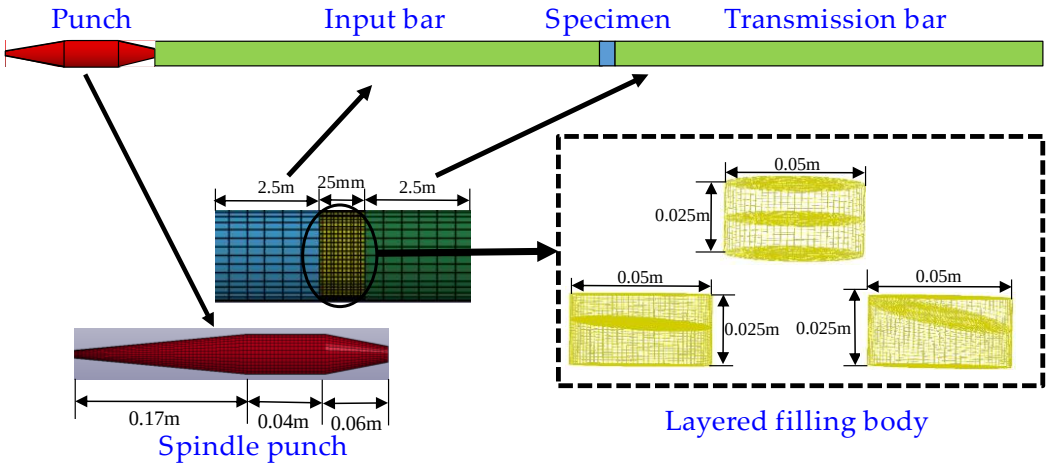

Figure 15. Establishment of a finite element model for a layered filling body.

5.2. Contact Definition and Boundary Conditions

Free surface contact was used between the spindle-shaped punch head and the incident rod. Erosion surface contact was adopted between the transmission rod and the test piece. Since there was a certain cohesive force between the two layers of the specimen, the force and the displacement between the layers of the filling body were transmitted through the cohesive force unit. The main method used was the binding contact method, and the failure parameters were set using the CONTACT_TIEBREAK_NODES_TO_SURFACE (8) contact type.

5.3. Material Model

According to previous research results, the cemented filling body is in principle a kind of low-grade concrete [28]. Holmquist, Johnson and Cook proposed a model called the HJC model [29] to deal with the problems of a high strain rate, large strain and high hydrostatic pressure in concrete. The model can be divided into three stages, as shown in Figure 16.

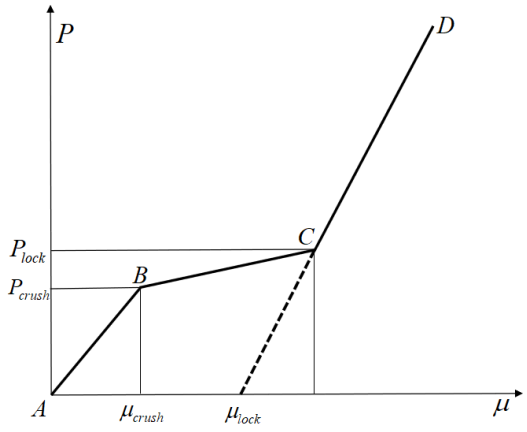

Figure 16. Equation of state curve of HJC.

First stage: this is the elastic stage (AB section), with $P \leq P_{\text{crush}}$ and elastic modulus $k_e = P_c/\mu_c$, where P is the hydrostatic pressure, P_{crush} is the actual pressure and μ is the volume strain of the specimen, and there is no obvious change in the micro-cracks and micro-pores in the concrete at this stage.

The second stage: this is the transition stage (BC section). At this time, $P_{\text{crush}} \leq P \leq P_{\text{lock}}$, and the internal micro-cracks and micro-pores of the concrete are gradually compacted, resulting in irreversible plastic deformation.

The third stage: this is the complete compaction stage (CD stage) when P reaches P_{lock}, and the micro-cracks and micro-pores in the concrete are completely compacted.

5.4. Selection of Material Parameters

According to the LS-DYNA Keyword Handbook, the HJC model contains 21 parameters, mainly basic mechanical parameters, damage parameters, pressure parameters and so on. However, it is difficult to obtain all of these parameters using experiments, such as the damage parameters D_1 and D_2 and the pressure constants K_1, K_2 and K_3. Therefore, in this paper, individual adjustment calculations were carried out on the basis of the parameters determined in a previous study [30], as shown in Table 3.

Table 3. HJC model parameters.

ρ (kg·m^{-3})	G/Pa	A/Pa	B/Pa	f_c/Pa	C/Pa	N/Pa	S_{max}
2000	5.57×10^7	0.35	0.85	3.00×10^6	0.01	0.61	7
T/pa	D_1	D_2	$\epsilon_{f,\,min}$	P_c/pa	μ_c	P_l/pa	μ_l
1.07×10^3	0.04	1	0.01	1.00×10^6	1.40×10^2	1.00×10^8	0.14
ε_0	FS	K_1/Pa	K_2/Pa	K_3/Pa			
1×10^{-6}	0.004	8.50×10^9	-1.7×10^{10}	2.08×10^{10}			

5.5. Simulation Analysis

5.5.1. Failure Mode Analysis of Layered Filling Body

Figure 17 shows the failure mode of a layered filling body with a cement–sand ratio of 1:4. The impact failure mode of a 0° layered filling body was studied when the impact velocity was 3.74 m/s (since the strain rate cannot be set by LS-DYNA, the failure mode of the layered filling body was studied using the impact velocity), with the extension of the impact time. Figure 17a shows that when t = 0.4 ms, the stress wave acting on the interface of the filling body continued to reflect through the specimen, leading to the first stress concentration in the filling layer near the end of the incident rod. It can be seen from Figure 17b that when t = 2.1 ms, the layered filling body was destroyed at the filling surface, resulting in the fracture of the specimen. Figure 17c shows that when t = 10 ms, the upper layer of the layered filling body was seriously damaged and the lower layer was mainly damaged at the filling surface.

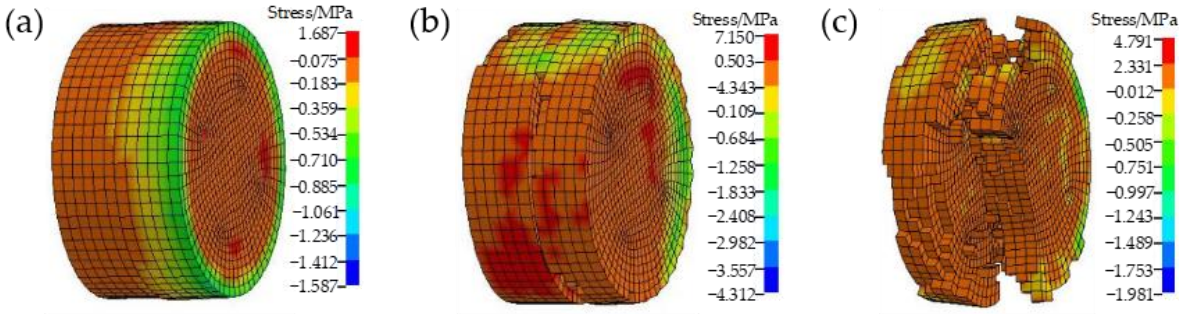

Figure 17. Stress distribution nephogram of 0° layered filling body: (**a**) failure time of 0.4 ms; (**b**) failure time of 2.1 ms; (**c**) failure time of 10 ms.

As shown in Figure 18a, the angle of the filling surface was set to be 13° and the cement–sand ratio was set to be 1:4. With the extension of the impact time, when t = 0.6 ms, the stress concentration of the layered filling body was first detected at the filling surface. As shown in Figure 18b, when t = 1.1 ms, the upper- and lower-layered filling body fractured along the filling surface, and the failure mode changed from splitting failure to shear failure. As shown in Figure 18c, when t = 9.4 ms, the lower layer of the filling body showed slight damage at the filling surface and the upper layer basically had no obvious damage, which was basically consistent with the failure process of Figure 14.

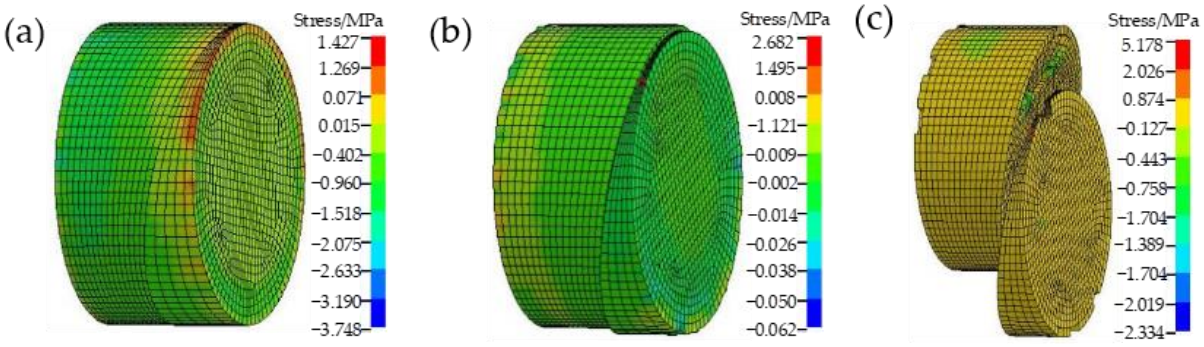

Figure 18. Stress distribution nephogram of 13° layered filling body: (**a**) failure time of 0.6 ms; (**b**) failure time of 1.1 ms; (**c**) failure time of 9.4 ms.

5.5.2. Analysis of Simulated Stress–Strain Curve of Layered Filling Body

As shown in Figure 19, the simulated stress–strain curve had stronger regularity than the experimental stress–strain curve. When the impact rate was 4.97 m/s and the filling surface angle was 0°, the dynamic peak strength of the layered filling body was 7.00 MPa. When the filling surface angle was 5°, the dynamic peak strength of the layered filling body was about 5.98 MPa. When the filling surface angle was 13°, the dynamic peak strength of the layered filling body was about 4.92 MPa, which was similar to the experimental peak strength. This indicates that the dynamic peak strength of layered backfill decreases gradually with the increase in the filling surface angle.

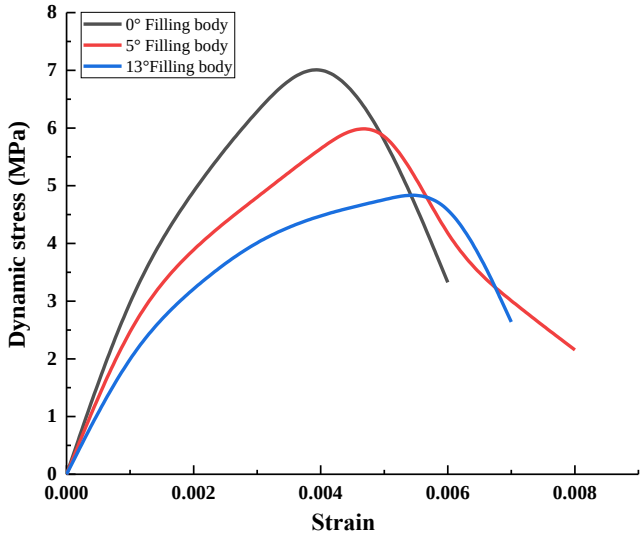

Figure 19. Stress–strain curves from the numerical simulation of the filling body at different angles.

6. Conclusions

In order to explore the dynamic characteristics of a layered filling body, this paper studied the influence of the filling surface angle, cement–sand ratio and strain rate on the dynamic peak strength, dynamic strength growth factor and failure mode of a filling body using the SHPB test system and LS-DYNA simulation software. The conclusions are summarized as follows:

(1) With the increase of the average strain rate, the dynamic peak strength and dynamic strength growth factor of the layered filling body increased gradually, and the dynamic strength growth factor of the layered filling body with the cement–sand ratio of 1:6 was greater than that of the filling bodies with the cement–sand ratios of 1:4 and 1:8.

(2) With the increase of the stratification angle, the static and dynamic peak strength of the layered filling body decreased gradually, and the higher the cement–sand ratio,

the higher the peak strength of the filling body was. There was no obvious change relating to the dynamic strength growth factor and the angle of the filling surface.

(3) According to the failure mode analysis and the LS-DYNA numerical simulation results for the layered filling body, with the increase in the stratification angle the failure mode of the layered filling body changed from splitting failure under tension to shear failure, and the dynamic peak strength of the filling body obtained in the experiment was similar to the dynamic peak strength of the filling body obtained in the simulation.

Due to the large difference in the wave impedance between the filling body and the steel rod, the amplitude of the transmitted wave of the filling body was much smaller than that of the incoming and reflected waves. Therefore, in subsequent research, the wave impedance between the filling body and the input and transmission rods (such as hollow rods or aluminum rods) could be reduced by replacing the rods and the amplitude of the transmission wave of the filling body could be improved.

Author Contributions: Conceptualization, J.L. and H.X.; methodology, Q.L. and M.Y.; writing—original draft preparation, J.L.; writing—review and editing and supervision, W.S., J.L. and S.C.; funding acquisition, W.S. and J.L. All authors have read and agreed to the published version of the manuscript.

Funding: This work was financially supported by the National Natural Science Foundation of China (Grant No. 51964023), Yunnan Fundamental Research Projects (Grant No. 202101BE070001-038; 202201AT070146; 202101BE070001-039), the National Key Research and Development Program (Grant No. 2019YFC1904202), the Yunnan Innovation Team Funding Project (202105AE160023) and the Yunnan Department of Education Science Research Fund Project (No. 2022J0055).

Data Availability Statement: Not applicable.

Conflicts of Interest: The authors declare no conflict of interest.

References

1. Jiao, H.; Chen, W.; Wu, A.; Yu, Y.; Ruan, Z.; Rick, H.; Chen, X.; Yu, J. Flocculated unclassified tailings settling efficiency improvement by particle collision optimization in the feedwell. *Int. J. Miner. Metall. Mater* **2022**, *44*, 553. [CrossRef]
2. Wu, A.; Ruan, Z.; Wang, J. Rheological behavior of paste in metal mines. *Int. J. Miner. Metall. Mater* **2022**, *29*, 717–726. [CrossRef]
3. Jiao, H.; Wu, Y.; Wang, H.; Chen, X.; Li, Z.; Wang, Y.; Zhang, B.; Liu, J. Micro-scale mechanism of sealed water seepage and thickening from tailings bed in rake shearing thickener. *Miner. Eng.* **2021**, *173*, 107043. [CrossRef]
4. Li, W.; Fu, Y.; Zhu, J. Research and Practice of Comprehensive Utilization Technology of Mine Water Based on Green Mining. *E3S Web Conf.* **2021**, *245*, 01007. [CrossRef]
5. Rania, R.; Joana, D.; Omar, D.; Mohamed, F.; Santos, B. A Tunnel under an In-Pit Mine Waste Dump to Improve Environmental and Landscape Recovery of the Site. *Minerals* **2021**, *11*, 566. [CrossRef]
6. Liu, X. Experimental Research on Support System of High Geostress Phyllite Tunnel. *Chin. J. Undergr. Space Eng.* **2021**, *17*, 1472–1478+1528.
7. Du, P.; Wang, Y. Investigation on Creep Characteristics of Rock-Like with Precast Internal Fissures under Different Temperatures and Confining Pressures. *Mater. Sci. Forum* **2021**, *6181*, 120–125. [CrossRef]
8. Wu, A.; Li, H.; Cheng, H.; Wang, Y.; Li, C.; Ruan, Z. Status and prospects of research on the rheology of paste backfill using unclassified tailings (Part 2): Rheological measurement and prospects. *Chin. J. Eng.* **2021**, *43*, 451–459. [CrossRef]
9. Yin, S.; Shao, Y.; Wu, A.; Wang, Y.; Chen, X. Expansion and strength properties of cemented backfill using sulphidic mill tailings. *Constr. Build. Mater.* **2018**, *165*, 138–148. [CrossRef]
10. Lan, W.; Wu, A.; Yu, P. Development of a new controlled low strength filling material from the activation of copper slag: Influencing factors and mechanism analysis. *J. Clean. Prod.* **2020**, *246*, 119060. [CrossRef]
11. Fang, K.; Fall, M. Shear Behavior of the Interface Between Rock and Cemented Backfill: Effect of Curing Stress, Drainage Condition and Backfilling Rate. *Rock Mech. Rock Eng.* **2020**, *53*, 325–336. [CrossRef]
12. Zhou, X.; Hu, S.; Zhang, G.; Li, J.; Xuan, D.; Gao, W. Experimental investigation and mathematical strength model study on the mechanical properties of cemented paste backfill. *Constr. Build. Mater.* **2019**, *226*, 524–533. [CrossRef]
13. Zhang, J.; Deng, H.; Taheri, A.; Deng, J.; Ke, B. Effects of Superplasticizer on the Hydration, Consistency, and Strength Development of Cemented Paste Backfill. *Minerals* **2018**, *8*, 381. [CrossRef]
14. Xu, W.; Li, Q.; Tian, M. Strength and deformation properties of polypropylene fiber-reinforced cemented tailings backfill. *Chin. J. Eng.* **2019**, *41*, 1618–1626. [CrossRef]
15. Cao, S.; Yilmaz, E.; Song, W. Fiber type effect on strength, toughness and microstructure of early age cemented tailings backfill. *Constr. Build. Mater.* **2019**, *223*, 44–54. [CrossRef]

16. Kesimal, A.; Yilmaz, E.; Ercikdi, B.; Alp, I.; Deveci, H. Effect of properties of tailings and binder on the short-and long-term strength and stability of cemented paste backfill. *Mater. Lett.* **2005**, *59*, 3703–3709. [CrossRef]
17. Xue, G.; Erol, Y.; Feng, G.; Cao, S.; Sun, L. Reinforcement effect of polypropylene fiber on dynamic properties of cemented tailings backfill under SHPB impact loading. *Constr. Build. Mater.* **2021**, *279*, 122417. [CrossRef]
18. Song, X.; Wang, S.; Wei, M.; Liu, W.; Wang, X.; Tao, T. Response of dynamic mechanical properties of alkali rice straw based cemented tailings backfill under SHPB impact load. *Chin. J. Nonferrous Met.* **2021**, *31*, 2583–2595. [CrossRef]
19. Cao, S.; Du, C.; Tan, Y.; Fu, J. Mechanical model analysis of consolidated filling pillar using stage-delayed backfill in metal mines. *Rock Soil Mech.* **2015**, *36*, 2370–2376. [CrossRef]
20. Wang, J.; Fu, J.; Song, W.; Zhang, Y.; Wang, Y. Mechanical behavior, acoustic emission properties and damage evolution of cemented paste backfill considering structural feature. *Constr. Build. Mater.* **2020**, *261*, 119958. [CrossRef]
21. Liu, E.; Zhang, Q.; Feng, Y.; Zhao, J. Experimental study of static and dynamic mechanical properties of double-deck backfill body. *Environ. Earth Sci.* **2017**, *76*, 689–696. [CrossRef]
22. Wang, J.; Fu, J.; Song, W. Mechanical properties and microstructure of layered cemented paste backfill under triaxial cyclic loading and unloading. *Constr. Build. Mater.* **2020**, *257*, 119540. [CrossRef]
23. Lu, H.; Liang, P.; Gan, D.; Zhang, S. Research on flow sedimentation law of filling slurry and mechanical characteristics of backfill body. *Rock Soil Mech.* **2017**, *38* (Suppl. 1), 263–270. [CrossRef]
24. Yang, B.; He, M.; Zhang, Z.; Zhu, J.; Chen, Y. A New Criterion of Strain Rockburst in Consideration of the Plastic Zone of Tunnel Surrounding Rock. *Rock Mech. Rock Eng.* **2022**, *55*, 1777–1789. [CrossRef]
25. He, M.; Zhang, Z.; Zhu, J.; Li, N. Correlation Between the Constant mi of Hoek-Brown Criterion and Porosity of Intact Rock. *Rock Mech. Rock Eng.* **2022**, *55*, 923–936. [CrossRef]
26. Li, X.; Gong, F. Research progress and prospect of deep mining rock mechanics based on coupled static-dynamic loading testing. *J. Coal Sci. Eng.* **2020**, *46*, 846–866. [CrossRef]
27. Hou, Y.; Yin, S.; Yang, S.; Zhang, M.; Liu, H. Study on the mechanical response and energy damage evolution process of cemented backfill under impact loading. *Rock Soil Mech.* 2021. [CrossRef]
28. Zhu, P.; Song, W.; Xu, L.; Wang, J.; Wan, F. A study on mechanical properties of cemented backfills under impact compressive loading. *J. Vib. Shock* **2018**, *37*, 131–137. [CrossRef]
29. Wang, Z.; Wang, H.; Wang, J.; Tian, N. Finite element analyses of constitutive models performance in the simulation of blast-induced rock cracks. *Comput Geotech* **2021**, *135*, 104172. [CrossRef]
30. Li, W.; Xu, J. Pulse shaping techniques for large-diameter split Hopkinson pressure bar test. *Acta Armamen Tarii* **2009**, *30*, 350–355.